ELSEVIER

MXene-enabled textile-based energy grid utilizing wireless charging

Alex Inman [a,b], Bita Soltan Mohammadlou [a], Kateryna Shevchuk [a], James FitzPatrick [a], Jung Wook Park [b], Noah Pacik-Nelson [b], Iryna Roslyk [a], Eric M. Gallo [b], Raghav Garg [c,d], Flavia Vitale [c,d,e,f,g,*], Andreea Danielescu [b,*], Yury Gogotsi [a,*]

[a] A.J. Drexel Nanomaterials Institute and Department of Material Science and Engineering, Drexel University, 3141 Chestnut St., Philadelphia, PA 19104, USA
[b] Accenture Labs, 415 Mission St. Fl. 34, San Francisco, CA 94105, USA
[c] Department of Neurology, University of Pennsylvania, Philadelphia, PA 19104 USA
[d] Center for Neuroengineering & Therapeutics, University of Pennsylvania, Philadelphia, PA 19104, USA
[e] Department of Bioengineering, University of Pennsylvania, Philadelphia, PA 19104 USA
[f] Department of Physical Medicine and Rehabilitation, University of Pennsylvania, Philadelphia, PA 19104 USA
[g] Center for Neurotrauma, Neurodegeneration, and Restoration, Corporal Michael J. Crescenz Veterans Affairs Medical Center, Philadelphia, PA 19104, USA

As the Internet of Things (IoT) expands, electronics will take on new form factors. With the ubiquity of textiles in our daily lives, integrating functionality into them is a promising proposition. Realizing a future with textile-based electronics (e-textiles) will require on-textile power supplies. Due to their high conductivity, electrochemically active surface, and ability to produce additive-free coatings from aqueous inks, MXenes are an ideal material to integrate into textiles to add functionality as well as generate and store electrical energy. Herein, we demonstrate an on-garment energy grid utilizing MXenes in textile-based supercapacitors and wireless chargers. Our on-garment energy grid can power real-world electronics, including peripheral electronics performing environmental sensing and data transmission, including an all-MXene surface electromyography (sEMG) sensor with real-time data transmission. Finally, we create a fully wireless textile-MXene joule heater directly powered by our MXene coil.

Keywords:MXene; $Ti_3C_2T_x$; e-textiles; Smart textiles; Antenna; Energy storage

Introduction

Textile-based electronics (e-textiles) are a rapidly growing and advancing technology that offer distinct benefits over traditional electronics in many applications due to their ubiquity, large surface area, and proximity to the user of textiles [1]. E-textiles provide flexible and lightweight wearable components for biomedical [2], athletic [3], human–computer interactions [4], and many other applications. The biggest area of emphasis has been on integrating functionality directly into a user's garments to provide a seamless collection of data without rigid components or additional devices to wear. Powering on-garment e-textiles for useful applications (e.g., heart rate monitoring and activity tracking) requires sufficient energy. While we have recently shown that such energy storage is possible in a textile form factor [5], there is the persistent problem of effectively delivering energy to on-garment energy storage without sacrificing user comfort. An effective on-garment energy grid is required to fully integrate and power e-textiles systems (Fig. 1a, b) [6].

There are several existing approaches to powering e-textiles. They can be plugged into the wall. However, this requires a hard/soft interface between wall power and the soft electronics

* Corresponding authors.
E-mail addresses: Vitale, F. (vitalef@pennmedicine.upenn.edu), Danielescu, A. (andreea.danielescu@accenture.com), Gogotsi, Y. (gogotsi@drexel.edu).

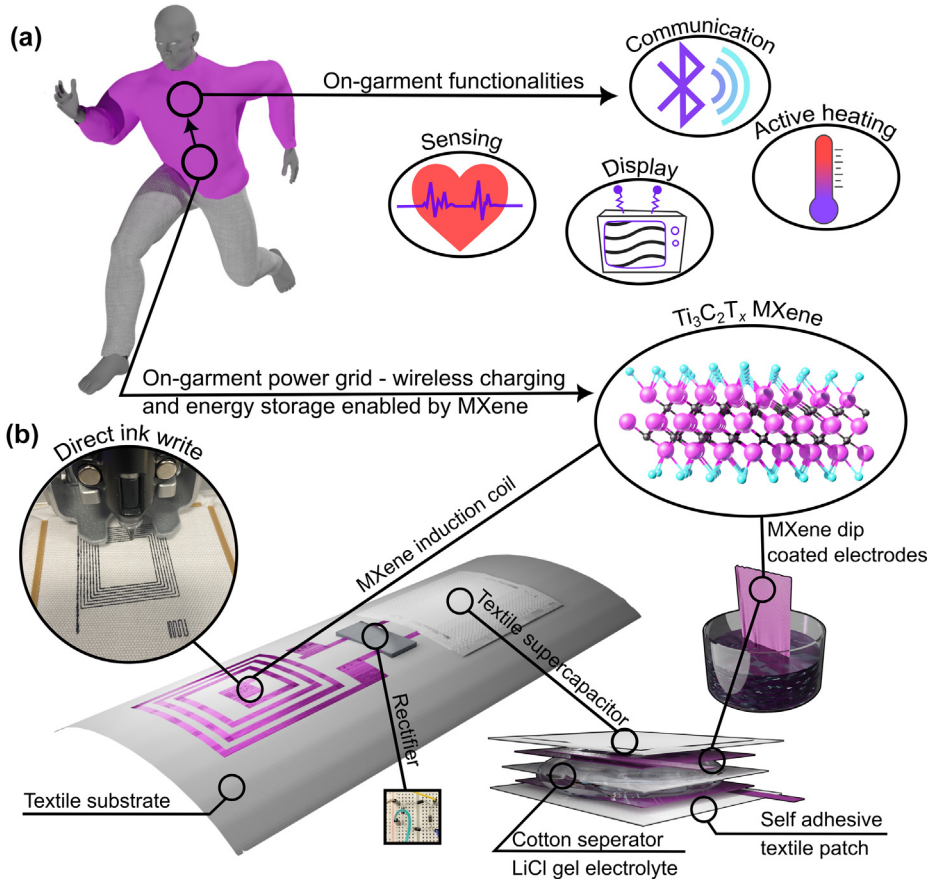

FIG. 1

a) Schematic depicting different possible applications and the need for on-garment power. **b)** a schematic depicting our solution. Integrating MXene-based wireless charging with MXene traces and MXene bond lines with applications and a MXene-textile supercapacitor.

in e-textiles. Direct power also restrains movement and does not provide the intended mobility and seamless integration of e-textile devices. These interfaces are prone to mechanical failure and can reduce user comfort due to their inherently rigid nature [7]. Another option is directly powering e-textiles with on-garment energy harvesting. Several energy harvesting approaches have been successfully integrated into textile form factors, each with advantages and disadvantages. Photovoltaic devices have been made in textile form factors with reasonable output, achieving currents from ~1–25 mA/cm^2, but with relatively low voltage limited by the PN junction's built-in voltage [8]. Additionally, photovoltaic textile devices have relatively complicated fabrication methods and require light to supply power. Piezoelectric and triboelectric nanogenerators have also been integrated into textiles. These devices generate a significant voltage (sometimes exceeding 100 V) but supply currents in the μA range [9,10]. Wireless charging through inductive power transfer offers substantial advantages over existing energy harvesting methods, supplying voltage and currents sufficient to power typical e-textile systems without needing a physical connector for power transfer. Charging or power delivery can be done on demand, using either a charging station at home or on the go, by inserting a transmitting coil into a pocket, for instance. Previous work has successfully integrated wireless charging into textiles by embroidery with silver yarn or screen printing of silver-polymer composite inks [11–13]. MXenes, directly integrated into textiles, offer an appealing alternative to making wirelessly powered e-textiles because MXene ink can be easily applied by direct-printing methods, adheres well to natural textiles, and can be dried at room temperature for a range of different applications. In contrast, thick film polymer inks contain hazardous solvents that may interact negatively with cellulosic substrates and require extended heating to drive off (>100 °C) [14]. Wearable applications do not typically require high power for operation, prioritizing user comfort and other factors.

MXenes are a family of two-dimensional (2D) carbides or nitrides with the formula $M_{n+1}X_nT_x$ where n = 1, 2, 3, or 4. M is an early transition metal, X is either carbon and/or nitrogen, and T is a surface termination bonded to the M element (e.g., OH, O, F, or Cl) [15]. The first discovered and most researched MXene, $Ti_3C_2T_x$ [16], has shown significant promise in textile-based applications [17,18]. $Ti_3C_2T_x$ is biocompatible, made of abundant chemical elements, is highly conductive (>20,000 S/cm) [19], and, due to its zeta potential in water (<−30 mV) [20], can be processed from an additive-free aqueous ink to form mechanically stable additive-free freestanding films and coatings on textiles. Due to its O/OH functionalized polar surface, $Ti_3C_2T_x$ adheres well to natural textiles (e.g., cotton) and can maintain functionality after multiple washing cycles [21]. MXenes can be

integrated into textiles at the fiber [22], yarn [23], and fabric [5] levels. Printing technologies like screen printing, ink-jet printing, and roll-to-roll techniques are potential methods to integrate electronic functionalities into textiles at a fabric level [24]. Due to MXenes' high anisotropy, aqueous MXene inks exhibit diverse rheological properties [25], allowing them to be deposited additive-free by various methods directly onto textiles at the fabric level to give patterned, functional designs by screen printing [26], ink-jet printing [22], and direct-ink-write printing (DIW) [27]. While each printing process has advantages and disadvantages, DIW allows for rapid prototyping and sufficient dry film thicknesses due to the rheological requirements and the relatively low volume percent of MXenes in aqueous MXene ink. Because MXene inks are a green water-based ink, MXene prints can be dried at room temperature directly onto textiles and add an array of functionalities, for example, energy storage [5], conductive interconnects [21], strain sensors [28], tactile sensors and haptic perception [29], surface electromyography sensing [30], joule heaters [28], antimicrobial garments [31], and wound healing [31].

Due to the advantages of MXene processing into textiles and the variety of functionalities that it can supply to textiles, we explore the multi-deposition, multifunctionality of MXenes directly interfaced with textiles and dried at room temperature. Specifically, we utilize DIW to print MXene induction coils (MX-coils), which act as receivers (R_x) for wireless power transfer, directly onto fabric substrates (Fig. 1b). We demonstrate the transfer efficiency's dependence on the number of turns and pitch and the effect of the transmitter coil's (T_x) properties on power transfer. A MXene coil is used to directly charge a MXene-textile supercapacitor, to power a microcontroller-based system to detect and transmit environmental data and surface electromyographic (sEMG) data and drive a fully wire-free MXene AC Joule heater. In doing so, we demonstrate the versatility of MXene in textiles by using it not just for printed T_x inductor coils but as the active material in a textile supercapacitor, a printed joule heater, a conductive trace, an electrical adhesive, and an electrode material for sEMG.

Results and discussion

MXene synthesis and characterization

For printing, we used aqueous dispersions $Ti_3C_2T_x$ MXene. MXene was synthesized using the protocol laid out by Downes et al. [32] To verify the successful synthesis of $Ti_3C_2T_x$, Raman spectroscopy, X-ray diffraction, and UV–Vis spectroscopy measurements were performed (SI 1a-c). The results from all three techniques match the literature data, signifying the successful synthesis of $Ti_3C_2T_x$ MXene [33–35].

Printing

Due to the high anisotropy of MXenes, they have a dramatic effect on the rheology of aqueous MXene inks; because of this, it is difficult to prepare and process inks above 50 mg/mL (~5 wt%) [25,36]. Due to the relatively low volume loading of MXene in aqueous MXene inks, printing techniques that use high-viscosity inks are ideal. The two most prominent approaches are screen printing and DIW printing. Screen printing is ideal for large-scale manufacturing, however, due to the relatively slow turnaround for producing screens of different patterns, it is not ideal for fast prototyping. DIW printing is a much slower application process, but design changes only require adjustments to software and design files. For this reason, DIW printing was best suited to the initial prototyping and development of the MX-coils.

Due to the demands of DIW printing, a rheological analysis was performed. The final ink formulation was approximately 50 mg/ml and 1100 nm (SI 1d). Fig. 2a–c shows a shear rate ramp, in which viscosity is tested with a series of higher shear rates. The MXene ink shows a relatively high viscosity at low shear rates but shows significant shear thinning (Fig. 2a). During DIW printing, there are several different shear rates – there is high shear through the needle but low shear as a deposited material on the substrate. As a shear-thinning material, MXene ink has low viscosity at high shear rates, allowing it to flow easily through the needle, but high viscosity at low shear, meaning that it retains its printed geometry without spreading on the substrate. Additionally, to a shear rate ramp, oscillatory tests were performed. An oscillation strain test was done to find the linear viscoelastic region (LVER) to run an angular frequency test and found that the ink had an LVER out to 0.1 % Fig. 2b. The ink showed a gel-like structure when we performed an angular frequency test at 0.1 % strain (Fig. 2c). The combination of high initial viscosity, high shear thinning, and a gel-like structure indicates that the ink is ideal for DIW printing [25,36].

Fig. 2d shows a basic schematic of DIW printing, in which a syringe filled with MXene ink is extruded through a needle as it moves along the designed path, which for our purposes is a MX-coil (Fig. 2e). We evaluated several different woven cotton substrates for the best print quality. Hydrophobic cotton (Fig. 2f), hydrophilic cotton (Fig. 2g), and hydrophilic cotton with a coarse weave (SI 2a-c). Coarsely woven hydrophilic cotton did not perform well. While the MXene wet the surface, the rough texture in both the x, y, and z directions led to inconsistent deposition and a higher frequency of short or open traces (SI 2a). With that in mind, hydrophobic and hydrophilic cotton with a finer weave were investigated (Fig. 2f, g). When comparing the x, and y dimensions in optical microscopy we find that the deposition appears very similar, however comparing the surface morphology of the two with nano-computed tomography (nanoCT), we can see that the hydrophobic prints are much less coherent, with a higher surface roughness when compared to the relatively smooth deposition of the MXene onto the hydrophilic sample (Fig. 2f, g).

Coil design

Initial coil designs were modeled in MATLAB using a conductivity of 20,000 S/cm and a thickness of 10 μm as assumptions for the MXene trace. The coils were then modeled against a 140 kHz T_x, a frequency within the range of the Qi standard [37] (further discussion can be found in SI 3). While modeling provided a solid design framework, due to practical limitations, primarily based on the surface roughness of the textile surface, many of the optimizing parameters had to be altered to accommodate the engineering challenges.

Supercapacitors and electronics (e.g., microcontrollers) primarily require DC power. Therefore, it is of primary importance

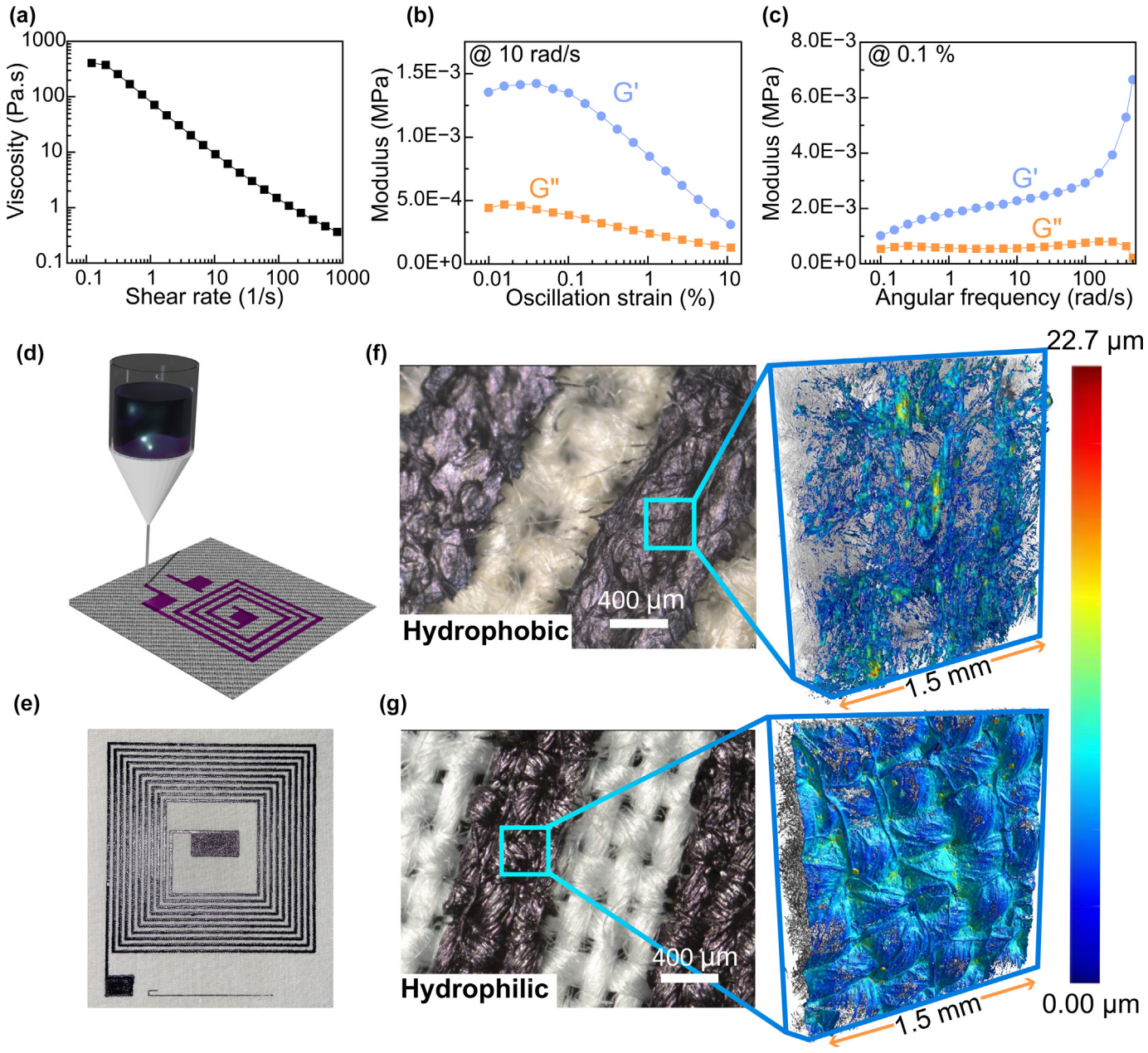

FIG. 2

Rheological data on a MXene ink. **a)** Shear rate ramp, **b**) amplitude sweep, and **c)** frequency sweep. **d)** Schematic depicting a direct-ink-write that is used to print wireless charging MXene coils. **e)** A photograph of a 5 × 5 cm^2 MX-coil. Light micrographs and nanoCT images of prints on **f)** hydrophobic and **g)** hydrophilic woven cotton, showing superior deposition onto hydrophilic cotton.

to test how efficiently the coils can produce DC power along with rectifying electronics. To test the effectiveness of MX-coils, we isolated several parameters such as shape, number of turns, and trace pitch (SI 4). To test how the geometric and printer parameters affected the DC output capabilities of the MX-coils we used the setup shown in Fig. 3b where a DC power supply fed power to a commercially available T_x coil. That coil then transferred wireless power to our MX-coil and subsequently into a full-bridge rectifier (4x 1N4007) before final measurements were taken with a multimeter. All MX-coils tested were packaged with an iron-on fabric patch (a consideration for real-world applications) as seen in SI 5. Additionally, the T_x module and rectifier used for these tests were not optimized for test results presented but a more optimized design based on energy harvesting ICs was implemented for powering devices, SI 6 and SI 7 discuss further the impact that different T_x modules and rectifier design can have on the final performance of the MX-coil. The final designs tested were 5 × 5 cm^2 rectangular coils with 10 turns and a pitch of 1200 µm (Fig. 2e) using T_x-1 (SI 6), and *R*-1 (a full discussion of the rectifiers can be seen in SI 7). It is important to note that while the MX-coils for powering the MXene-textile supercapacitor and microcontrollers were created according to the design laid out in Fig. 3a, direct current (DC) analysis was done with coils that had copper tabs connected to the pads.

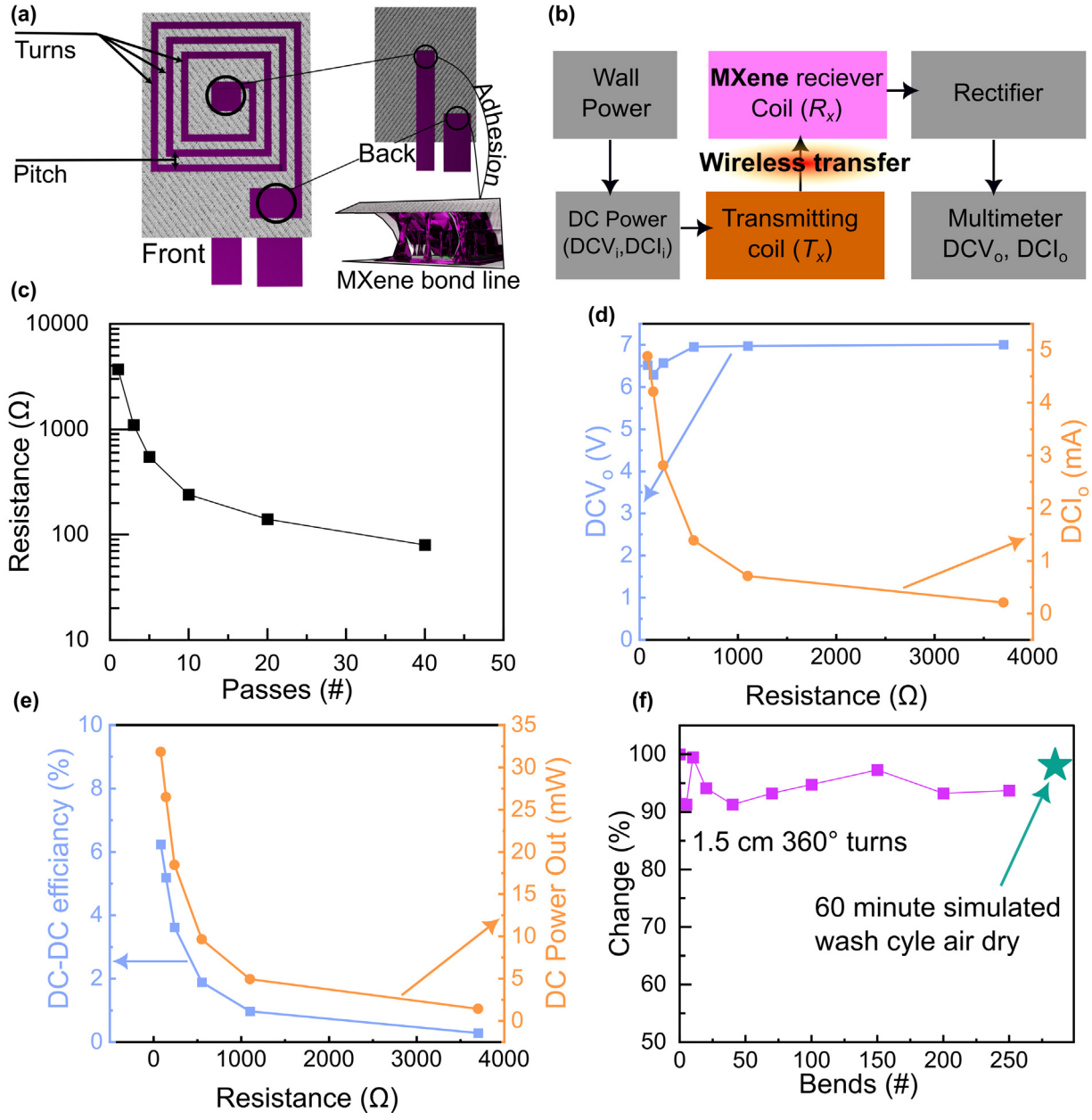

FIG. 3

a) Schematic of MXene coil design. **b)** Diagram for testing DC output of MXene coils. **c)** DC resistance as a function of print passes on a final design. **d)** DCV$_o$ and DCI$_o$ as a function of DC resistance and **e)** and DC power out and DCV$_o$ to DCV$_i$ efficiency as a function of resistance. **f)** The change in power output as a function of 250 bending cycles and a 60-minute simulated wash cycle at 60 °C and 360 RPM.

Initial tests showed that almost all coil versions delivered the necessary voltage levels under standard transmission signals (39 Vpp at 105 kHz) and an open circuit load measured by placing the packaged MX-coil directly onto the T_x coil (17 Vpp at 102 kHz). Significant differences were seen, however, between coils in overall power delivery, with parasitic resistance reducing the ability to reach necessary power levels for typical on-body electronics use. To establish the overall relationship between coil resistance and maximum power, we increased the number of printing passes over the coil design, thereby increasing the MXene trace thicknesses and reducing parasitic resistance (Fig. 3c). We tested six samples with 1–40 passes on a coil with 10 turns and 1200 μm pitch. While we see a relatively small voltage dependence on coil resistance, we see a significant increase in the DC output current (DCI$_o$) with decreasing resistance (Fig. 3d). This, in turn, leads to higher DC-DC efficiency and DC power output (Fig. 3e). The objective was to find the minimum thickness necessary to deliver reasonable power for the applications demonstrated. While it is difficult to measure the dry film thickness on a textured substrate such as textiles, the final mass of our MX-coils is under 100 mg, which is significant when compared to a standard copper R_x, which is over 4.0 g, making the MX-coil > 40X lighter than its copper counterpart.

Finally, to evaluate the MX-coils as wearable devices, we tested mechanical properties meant to simulate real-world use. Mechanical testing was done by bending the sample 360° (180°

one way and then 180° in the reverse direction) around a 1.5 cm diameter dowel (SI 8a, b). We found that the MX-coils delivered 92 % of initial DC output power after 250 cycles (Fig. 3f), deviations in the bending data may be due to inconsistent registration of the T_x coil with the MX-coil. After 250 cycles of bending were performed, a simulated washing cycle was done on a hot plate at 60 °C and RPM of 360 (SI 8c) and then air dried for 24 h. After the simulated wash, we found that the coil delivered an average of 99 % of the original DC power output (Fig. 3f). In addition to the simulated wash, we also tested how effectively the MX-coil provided power while being bent (SI 9). We bent the MX-coil around dowels of different sizes (SI 8a) and found that it retained 20 % efficiency down to 1.5 cm, and 75 % efficiency at 6 cm (a more realistic diameter for real-world situations, like bending around a leg) (SI 9a). It is important to note that the T_x coil is still rigid in this experiment, producing a larger distance between the T_x coil and the MX-coil at the edges as the diameter of the dowel decreases. While most of this work is focused on using commercially available T_x coils, we also investigated using an MX-coil as a T_x to demonstrate that it could be used to supply power as well as transmit information. SI 9b shows that when coupling MX-coils as both T_x and R_x we found a resonant frequency of 15 MHz when rectifying the AC power through a power management board (*R*-2), supplying 40 mW at 3.3 V. We were also able to demonstrate simple ASK and FSK communication between the coils but neither T_x or R_x were coupled to a capacitive element and the large resonant frequency is attributed to parasitic capacitances present in the circuit. Further circuit design can reduce the operating frequency to typical ranges. The commercially available copper coils that we used operate well under this frequency at 70 kHz, 100 kHz, and 140 kHz for T_x-1, T_x-2, and the Qi protocol charger. Preliminary experiments also demonstrated that ferrite backing on the receiver can significantly increase efficiency (~2x) but this was not included in testing as ferrite cannot be easily integrated with practical devices.

Integration of MX-coil with MXene-textile supercapacitor

While we have shown that textile-based wireless charging is possible using MXene, an on-garment energy grid capable of powering complex electronics requires a device capable of storing the energy. We developed an MXene-textile supercapacitor consisting of MXene-coated non-woven cotton textile electrodes, a non-woven cotton textile separator, and LiCl PVA-water gel electrolyte (Fig. 5a). Each cell is then encapsulated in Kapton tape and placed within a sandwich of waterproof self-adhesive textile patches, the final device has three cells in series, capable of charging to 3.3–3.6 V (Fig. 5a).

To construct the MXene-textile electrodes, non-woven cloth (Fig. 4a) was dipped into aqueous MXene solution until the MXene loading was approximately 78 %. To improve upon our previous work [5], we tested two different sizes for infiltration, 920 nm (labeled MXene-large: MX-L) and 380 nm (labeled MXene small: MX-S) (Fig. 4b), with conductivities of 10,000 S/cm and 4,000 S/cm respectively. SEM images of the top and cross-sectional nanoCT of MX-L (Fig. 4c, d) and MX-S (Fig. 4e, f) coated non-woven cotton, both with 78 % MXene by weight, show the effect of MXene flake size on how it absorbs into the fabric. MX-L dip-coated samples show a consistent outside coating from SEM but are less able to penetrate and coat individual fibers (Fig. 4c, d), while MX-S coated samples show a porous structure

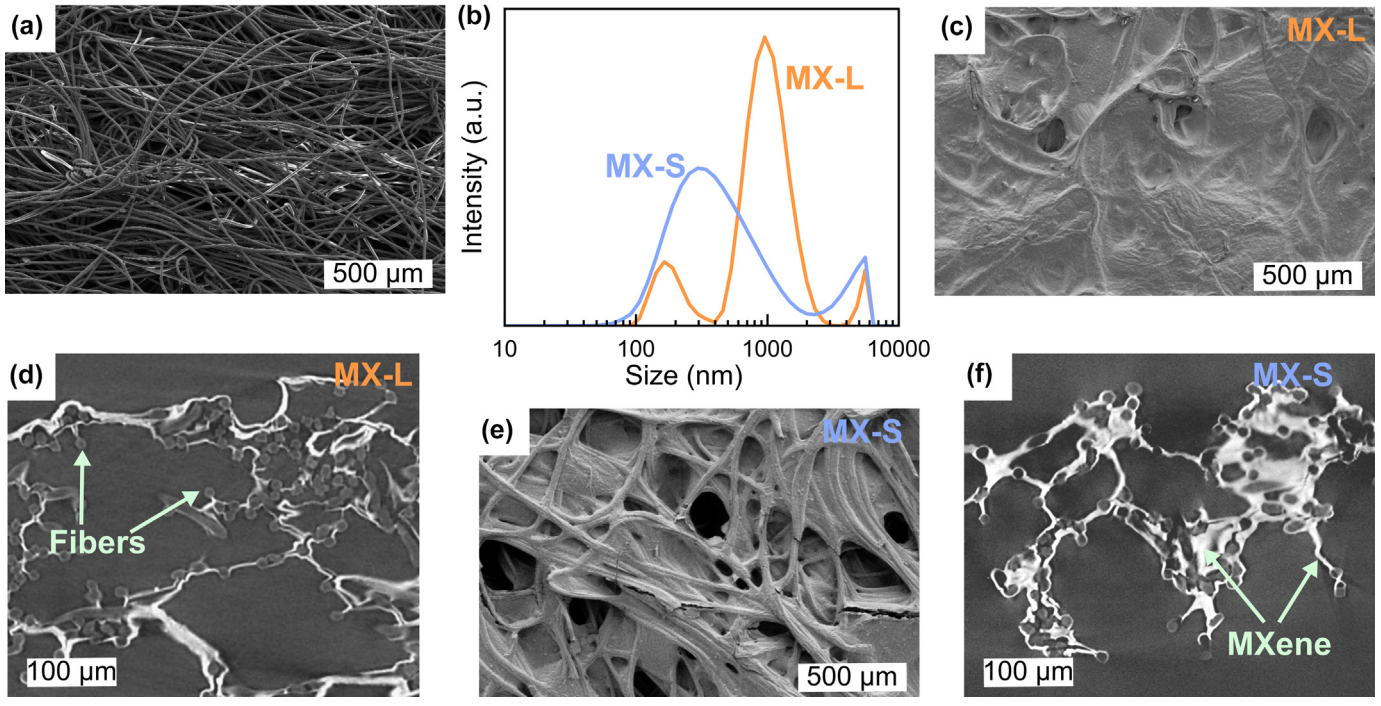

FIG. 4

a) SEM image of uncoated non-woven cotton textiles. **b)** DLS analysis of large (MX-L) and small (MX-S) MXenes. **c)** SEM image of the top and **d)** nanoCT image of the cross-section of non-woven cotton textiles coated in MX-L. **e)** SEM image of the top and **f)** nanoCT image of the cross-section of non-woven cotton textiles coated in MX-S.

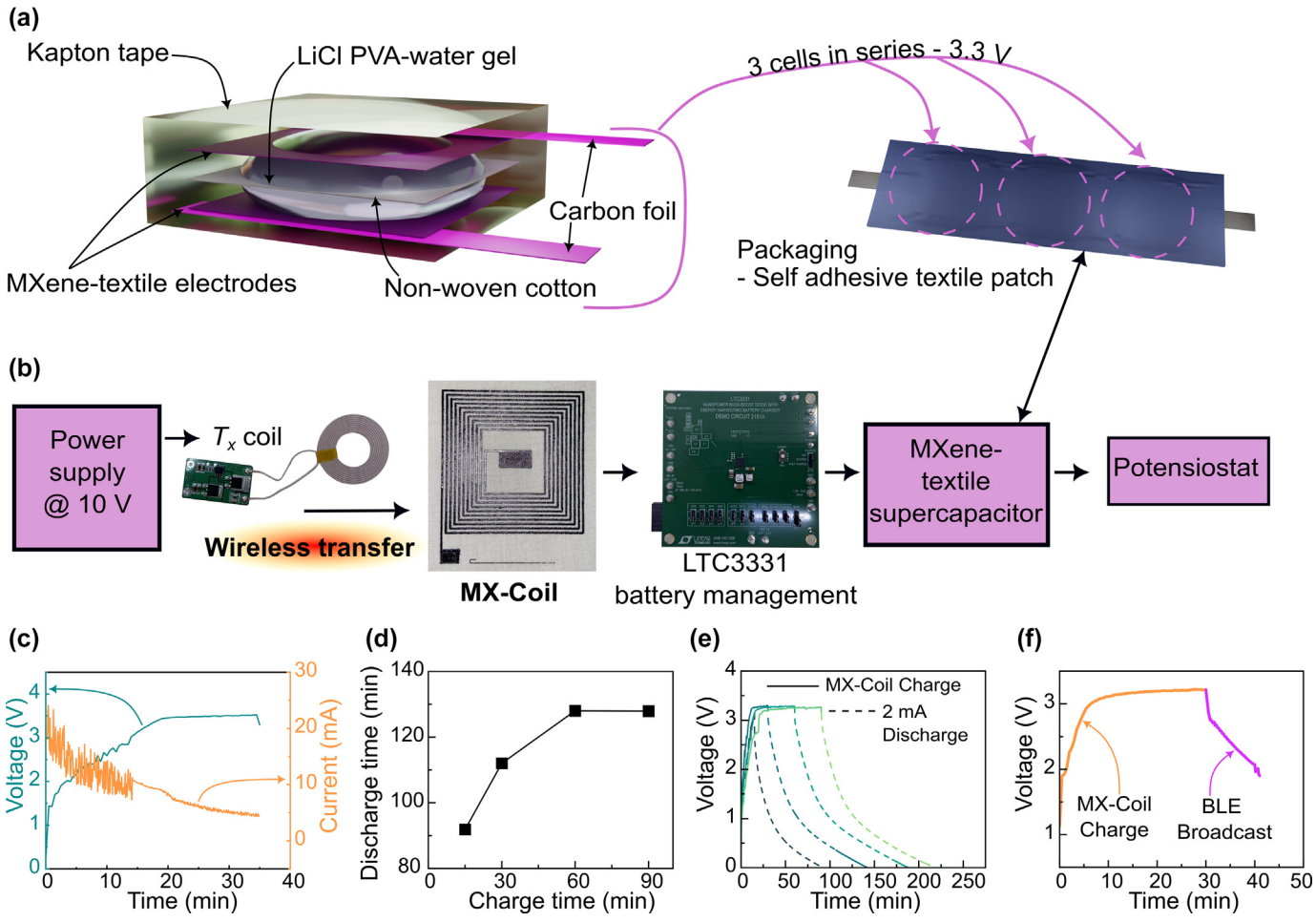

FIG. 5

a) Schematic of MXene-textile supercapacitor that is being powered by the MX-coil. **b)** Schematic of testing setup. **c)** Curves of MX-coil charge and 2 mA discharge. d) Discharging time at 2 mA as a function of MX-coil charging time. **e)** MX-coil charging current and MXene-textile supercapacitor voltage. **f)** Powering an Artemis Nano microcontroller for BLE broadcast with MXene-textile supercapacitor charged with MX-coil.

on the outside but MXene coating individual fibers throughout the cotton substrate (Fig. 4e, f). While this may seem to indicate better kinetics for ion insertion and de-insertion MX-S coated samples, smaller flakes equate to lower conductivity, and as a result, we observe a significant *IR* drop in MX-S coated samples that is not present in the MX-L coated samples (SI 10a, b). For this reason, MX-L-coated samples are tested when charging with an MX-coil. While further analysis of the stand-alone MXene-textile supercapacitors can be found in SI 10 one concern is the lifetime of the devices. While MXene-based supercapacitors have shown long cycle life, up to 500,000 cycles [38], when tested in ideal Swagelok cells, the relatively complicated engineering of the MXene-textile supercapacitors led to some concern. We saw significant degradation of the cell over time; however, we could "reconstitute" the cell by squishing it under approximately 10 kg for several hours (SI 10c, d). This leads us to believe that we are losing contact between our carbon foil tabs and the MXene-textile electrodes rather than observing a breakdown of the electrodes themselves. A future area of study for textile-based supercapacitors is the packaging, and this problem could be mitigated by packaging supercapacitors in pre-strained packaging materials that will compress the devices under tension.

An MX-coil was fabricated with a pitch of 1200 μm, 10 turns, and 40 passes (resistance = 80 Ω) to analyze how effectively MX-coils can charge MXene-textile supercapacitors capable of powering on-body electronics and transmitting data via Bluetooth. The testing diagram can be seen in Fig. 5b; in short, a DC power supply feeds 10 V into T_x-2, where power is transferred wirelessly to the MX-coil, AC power is then diverted through a battery management system that rectifies the signal and limits the voltage going into the supercapacitor (R-1). The charging is collected on a potentiostat, while voltage data is collected by measuring the voltage at the supercapacitor terminals, and the current data is collected in series between the LTC3331 power management board and the supercapacitor.

Fig. 5c shows the current being supplied by the MX-coil to the MXene-textile supercapacitor and the corresponding voltage of the supercapacitor. We observe a voltage plateau obtained in under 20 min, however, there is still residual current being supplied, indicating that the supercapacitor is not being fully charged. To investigate this further, we charged the supercapacitor with the MX-coil at different times and monitored the discharge times with a 2 mA draw (a typical current for a microcontroller module (SI 11)) (Fig. 5d, e). From this data, we

see 90-minute discharge times after 15-minute charging and a plateau of discharge times after 60 min of charging, indicating that the MXene-textile supercapacitor is fully charged. Finally, to demonstrate the applicability of this design, we charged the MXene-textile supercapacitor with the MX-coil. We then disconnect the MX-coil and power an Artemis Nano microcontroller with constant BLE broadcast (Fig. 5f). After 30 min of charge, our MXene-textile supercapacitor can power constant BLE broadcast for 13 min (Fig. 5f). It is important to note that constant BLE broadcast is a high power operation of the system and that by optimizing the energy consumption for the specific application, operation time can be significantly extended [5].

Standalone applications

Beyond on-garment applications requiring energy storage, we also demonstrated use cases that may not require energy storage. For example, situations with relatively stagnant users, such as a baby in a crib or a patient in a hospital bed, may allow direct power applications without the need for on-garment energy storage, which may add complexity to the design. To validate this, we demonstrate several different applications using power from the MX-coils directly.

We implemented a platform to record human neuromuscular activity using wearable MXene-based electrodes (MXtrodes) and power a wireless EMG sensor (Fig. 6a). Here, we place a bipolar assembly of wearable bipolar MXtrodes onto the skin over the biceps of a healthy participant (for details regarding the fabrication of the MXtrodes, sEMG sensor, and the sEMG data acquisition see Materials and Methods). Our wearable MXene electrodes can be easily customized to fit any target anatomy and do not require specialized skin preparation or conductive gels to enable non-invasive recordings of human electrophysiology [30,39]. We acquired real-time sEMG activity of the biceps in a bipolar configuration as the participant performed maximum voluntary contractions of the biceps with a high signal-to-noise ratio (SNR) of 8.1 ± 0.1 dB (Fig. 6b) using only wireless power transmitted to our MX-coils. This demonstrates the feasibility of having an all-MXene platform for powering wearable electronics and acquiring relevant human electrophysiological data non-invasively in time.

In addition to sEMG with MXene electrodes, we also demonstrated the MX-coils ability to power a standard wireless sensing application using off-the-shelf hardware. For this, we monitored temperature and humidity measurements with built-in sensors on an Arduino Nano IoT board being powered directly by an MX-coil through a rectifier using human breathe and a hair dryer as inputs to the sensors (Fig. 6c). Data is collected and transmitted wirelessly using a Bluetooth connection. Finally, we demon-

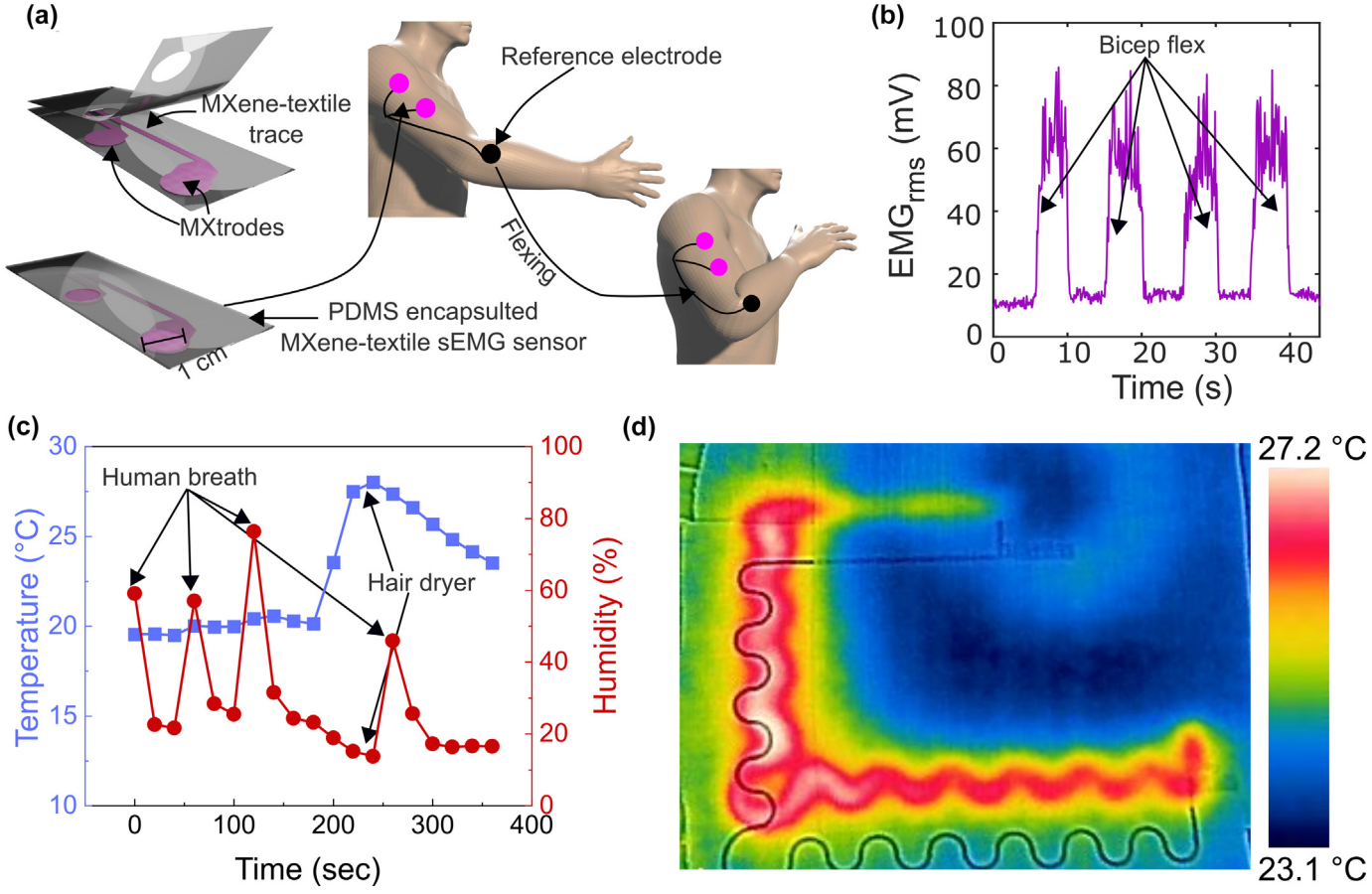

FIG. 6

a) Schematic of MXene-textile electrodes and bicep flex. **b)** RMS sEMG of flexing bicep collected by MXene-textile electrodes directly powered by MX-coil. **c)** Breath sensing data collected off of an Arduino Nano IoT microprocessor powered directly from the MX-coil. **d)** An all-MXene Joule heater that uses an MX-coil to heat an MXene AC joule heating trace printed onto the textile.

strated an AC joule heater directly powered by the MX-coil without any rectifier (Fig. 6d) with the full system consisting of only MXene and textile, using a MXene paste to make electrical contact between the MX-coil (90 Ω) and the printed MXene heating element (820 Ω). We see a relatively modest temperature gain of 4.1 °C (Fig. 6d) in an unoptimized proof-of-concept, and that, along with optimizing the MX-coil, the ratio of resistances between the low resistance MX-coil and the higher resistance heating element can help improve heating. This device requires no rectification and is a fully standalone, wire-free heating device that can powered externally and is made with only MXene and textiles. Additionally, in principle, this device could be scaled to larger areas and be powered by a battery with T_x capability (i.e., a cell phone in a pocket could wirelessly power a textile-based joule heater) that requires no hard/soft interface and could be easily removed for washing of a garment.

As this work has demonstrated, there is great potential to advance society by adopting e-textiles, from enhanced healthcare to streamlining human–computer interactions. There are a large number of examples of effective e-textile sensors and components. Addressing the issues related to power allowed us to create practical, commercially viable systems.

Conclusions

By taking advantage of the unique properties of MXenes, we have produced a textile-based wireless charging system that enables wireless power injection into e-textile systems by printing $Ti_3C_2T_x$ MXene induction coils directly onto fabrics. We demonstrate its effectiveness in powering several relevant e-textile uses and power transfer up to 10 % efficiency, resulting in 100 mW of power directly applied to textiles. We also used it to charge a MXene-textile supercapacitor, introducing the idea of an on-garment energy grid fully made of MXene. This energy grid is shown to be able to power standard electronics for on-body sensing and wireless transmission of data. Additionally, we show that MX-coils are capable of directly powering MXene-based sEMG sensors with wireless live data transmission. Finally, we demonstrate a proof-of-concept all-MXene, all-textile AC Joule heater containing no hard-soft interfaces. These initial demonstrations provide a baseline of what is possible using MXene textile induction coils for wireless energy transfer. Further work is needed to optimize the full receiver/transmitter design to create resonant behaviors and potentially add other materials to increase efficiency.

Materials and methods

Ti_3AlC_2 MAX phase synthesis

TiC powder (99.5 %, −325 mesh, Alfa Aesar, USA) and aluminum powder (99.5 %, −325 mesh, Alfa Aesar, USA) were mixed with coarse titanium sponge (60–325 mesh, Pyro Chemical Source LLC) in molar ratios 2TiC:2.2Al:1.25Ti, providing an excess of aluminum. The mixing was performed in a ball mill using zirconia beads at 70 rpm for 18 h. A 2:1 mass ratio of zirconia milling beads to the precursor powder mixture was used. The homogeneous mixture was cold pressed in a stainless-steel mold with a pressure of 1000 psi to form a pellet with a diameter of 28 mm.

The sintering of pellets was carried out in a GSL-1700X tube furnace (MTI Corporation, USA) at 1400 °C for 2 h in argon flow. The heating and cooling rates were both 3 °C/min. The sintered pellets of Ti_3AlC_2 were crushed into powder manually. For removing impurities, such as intermetallics and oxides, the produced powder was sieved to less than 38 μm particle size and washed in 9 M HCl for 20 h at room temperature while stirring. The washed and dried Ti_3AlC_2 was used to produce $Ti_3C_2T_x$.

MXene synthesis

MXene $Ti_3C_2T_x$ was synthesized by selective wet-chemical etching. One gram of prepared Ti_3AlC_2 MAX phase was immersed in 20 mL of etchant and stirred at 300 rpm at 35 °C for 24 h. The etching solution contains a mixture of HF (Acros Organics, Fair Lawn), HCl (Hydrochloric acid, Fisher Scientific), and DI water with a volumetric ratio of HF:HCl:H_2O equal to 1:6:3. Multilayered $Ti_3C_2T_x$ MXenes were intercalated with LiCl (Lithium chloride, 99 %, Alfa Aesar) using 1 g of LiCl per 1 g of Ti_3AlC_2 MAX, dissolved in 50 mL of DI water, and stirred at 300 rpm at room temperatures for 24 h.

The resulting solution was washed with DI water and centrifuged at 3500 rpm for 5 min. The supernatant was discarded, and the delaminated MXenes were redispersed by manual shaking. The washing cycles were repeated until the supernatants reached pH 6. Then, the colloidal solution was centrifuged at 3500 rpm for 60 min, and the supernatant containing single layer $Ti_3C_2T_x$ was collected.

Rheology:

Rheological measurements were performed using a TA Instruments Discovery HR-3 rheometer with a 20 mm parallel plate at 25 °C and a 0.5 mm gap distance.

Direct ink write (DIW) printing:

Direct-ink-write printing was done on a Voltera V-one. The syringe was a 250 μm ID, 500 μm. Raster speeds varied from 1 mm/s to 600 mm/s.

NanoCT analysis:

The MXene distribution inside the coated textiles was assessed using a Nano-CT system (Zeiss Xradia 620 Versa, California, U.S.), operating at a voltage of 60 kV and a power of 6.5 W. The system featured a 4X detector, achieving spatial resolutions of 0.75 μm for printed samples and 0.9 μm for deeply coated samples. During the scan, a total of 4210 projection images were captured, employing an LE2 filter to minimize noise and enhance image clarity. Post-acquisition, these images were processed with Zeiss XRM reconstructor software (California, U.S.), applying adjustments for center shift and beam hardening to ensure precise imaging. Further image enhancement involved Gaussian filtering to refine segmentation quality. Segmentation and quantitative analysis were conducted with ORS Dragonfly Pro software, using a thresholding method enhanced by manual adjustments for better accuracy. This quantitative analysis specifically measured the thickness and uniformity of the MXene coating on the textile.

Scanning electron microscopy (SEM):

SEM was performed using a Thermo Fisher Apreo 2S Lo Vac scanning electron microscope at an operating voltage of 5 kV voltage and beam current of 0.20 nA. Images were captured using a secondary electron (SE) detector at magnifications from 120x to 15,000x.

Optical microscopy:

Optical microscopy was performed using a Keyence VK-X1050 microscope.

Raman spectroscopy:

A confocal Renishaw inVia Raman spectrometer in inverted reflection mode was used for all measurements. All free-standing films were measured using a 785 nm laser with 1200 line/mm grating, an excitation intensity of 3.59 mW × 10 %, the 30 s acquisition time, and the × 63 objective (NA = 0.7).

UV-Vis spectroscopy:

An Evolution 201 UV–Vis spectrometer was used to collect spectra in transmission geometry across 1000–200 nm from dilute MXene suspensions in a quartz cuvette with a 10 mm optical path.

Dynamic light scattering (DLS):

Size measurements were performed on dilute MXene suspensions using a Malvern Zetasizer Nano ZS. A refractive index of 2.15 for Ti metal was used for measurement calculation.

X-ray diffraction (XRD):

A Rigaku SmartLab was used at 40 kV and 30 mA with CuK_α X-ray radiation with Bragg-Brentano geometry at 2θ = 3°-70°, a step scan of 0.01°, and a step time of 1 s.

Infrared measurement:

Infrared measurements were done with a FLIR E8xt (USA) infrared camera.

Wireless charging:

Three transmitter coils were used: Adafruit Inductive Charging Set – 3.3 V @ 500 mA (T_x-1) max, Adafruit High Current Inductive Charge Kit – 5 V at 1.3 A max (T_x-2), and a standard Qi charger. For DC conversion a full bridge rectifier (4x 1N4007 diodes) and a LTC3331 nanopower buck-boost DC/DC with energy harvesting battery charger DC2151A evaluation board were attached to the receiver coil output. The receiver circuit was not optimized to achieve resonance at the transmitted frequency.

MXtrode fabrication:

The sEMG electrodes were fabricated following our previously published protocol.[1,2] Briefly, a cellulose-polyester textile (60:40 blend, Texwipe TexVantage) was laser cut using a CO_2 laser (Universal Laser Systems PLS 4.75) following a computer-aided design of the desired bi-polar electrode geometry. The laser-cut textile was attached to a thin film of 1:10 polydimethylsiloxane (PDMS, Sylgard 184) using a medical adhesive spray (Skinister). The textile was then infused with 20 mg/mL $Ti_3C_2T_X$ MXene and dried in an oven at 80 °C for 1 h. Backend pin connectors (FCI/Amphenol FFC) were attached using Ag epoxy (CW2400 CircuitWorks). A top passivation of polydimethylsiloxane was applied as a thin film. After curing the top PDMS at 80 °C for 1 h, the electrodes were exposed using a 10 mm biopsy punch.

Wireless EMG sensor:

The wireless EMG sensor was assembled onto a customized printed circuit board (PCB) [40]. A commercially available chipset, ADS 1293 analog front end (Texas Instruments), was used as a differential amplifier and an analog-to-digital converter to record EMG signals in a bipolar configuration. The digital data from the ADS1293 was transmitted to a microcontroller (Xiao nRF52840, Seeed Studio). The microcontroller implemented a real-time digital high-pass filter with a cut-off frequency of 10 Hz on the raw bipolar EMG recordings. The RMS of the filtered bipolar EMG signals was also computed in real time using a sliding window over 50 data points without overlap. The RMS_{EMG} data was then transmitted using Bluetooth-low-energy (BLE) to a receiving terminal (Xiao nRF52840, Seeed Studio) connected to a controller.

sEMG data acquisition. Prior to placing the bipolar MXtrode electrodes onto the biceps of a healthy participant, the skin was cleaned with an alcohol wipe. The MXtrode was then placed on the arm with one of the electrodes over the bicep muscle belly and the other on the distal end. A commercially available gelled Natus electrode was placed on the bony part of the wrist as the reference electrode. All electrodes were connected to the corresponding terminals on the custom sEMG sensor. sEMG data was then acquired at 533 Hz, and the incoming RMS_{EMG} data was read and plotted in real time using MATLAB.

The signal-to-noise ratio (SNR) of the sEMG data was calculated using the following equation-

$$SNR = 10 * \log_{10}\left(\frac{\max\left(RMS_{signal}\right)}{\max\left(RMS_{noise}\right)}\right)$$

CRediT authorship contribution statement

Alex Inman: Writing – review & editing, Writing – original draft, Visualization, Validation, Software, Project administration, Methodology, Investigation, Formal analysis, Data curation, Conceptualization. **Bita Soltan Mohammadlou:** Writing – review & editing, Visualization, Methodology, Investigation, Formal analysis, Data curation. **Kateryna Shevchuk:** Writing – review & editing, Validation, Software, Methodology, Investigation, Formal analysis, Data curation. **James FitzPatrick:** Writing – review & editing, Visualization, Validation, Software, Methodology, Formal analysis, Data curation. **Jung Wook Park:** Validation, Software, Methodology, Investigation. **Noah Pacik-Nelson:** Validation, Software, Methodology, Investigation. **Iryna Roslyk:** Writing – review & editing, Methodology, Formal analysis. **Eric M. Gallo:** Writing – review & editing, Writing – original draft, Validation, Supervision, Project administration, Methodology, Investigation, Formal analysis, Data curation, Conceptualization. **Raghav Garg:** Writing – review & editing, Software, Methodology, Investigation, Conceptualization. **Flavia Vitale:** Supervision, Funding acquisition. **Andreea Danielescu:** Writing – review & editing, Supervision, Investigation, Funding acquisition. **Yury Gogotsi:** Writing – review & editing, Writing – original draft, Supervision, Resources, Project administration, Investigation, Funding acquisition, Conceptualization.

Data availability

Data will be made available on request.

Declaration of competing interest

The authors declare that they have no known competing financial interests or personal relationships that could have appeared to influence the work reported in this paper.

Acknowledgements

We would like to thank John Atkinson at the Accenture Garage for his hospitality, help, and design of a stage for printing onto textiles, and Kyle Matthews for providing MXene. Roman Rakhmanov for assistance with MATLAB. XRD, and SEM analyses were done with instruments in the Materials Characterization Core at Drexel University. Nano-CT analysis was conducted at the Materials Characterization Core at Drexel University supported by MRI award number 2216175 (B. S. M.). The authors would like to acknowledge funding support from the National Institutes of Health (NIH Award No. R01AR081062 to F.V.) and Accenture, LLP.

Appendix A. Supplementary material

Supplementary data to this article can be found online at https://doi.org/10.1016/j.mattod.2024.10.008.

References

[1] W. Weng et al., Angew. Chem. Int. Ed. 55 (2016) 6140–6169.
[2] G. Chen et al., Chem. Rev. 122 (2022) 3259–3291.
[3] D. Vieira, H. Carvalho, B. Providência, J. Biomimetics Biomater. Biomed. Eng. 57 (2022) 37–46.
[4] S. Liu et al., Adv. Funct. Mater. 31 (2021) 2007254.
[5] A. Inman et al., J. Mater. Chem. A 11 (2023) 3514–3523.
[6] L. Yin et al., Nat Commun 12 (2021) 1542.
[7] Y. Khan et al., Adv. Funct. Mater. 26 (2016) 8764–8775.
[8] A. Rafique et al., Nano-Micro Lett. 15 (2023) 40.
[9] S. Bairagi et al., Nano Energy 111 (2023) 108414.
[10] R. Walden et al., Chem. Eng. J. 451 (2023) 138741.
[11] D. Sun et al., J. Ind. Text. 50 (2020) 333–345.
[12] M. Wagih et al., IEEE Trans. Ind. Electron. 71 (2024) 3741–3750.
[13] L.R. Clare et al., J. Phys.: Conf. Ser. 660 (2015) 012135.
[14] T. Blachowicz, G. Ehrmann, A. Ehrmann, Macromol. Mater. Eng. 308 (2023) 2200692.
[15] A. VahidMohammadi, J. Rosen, Y. Gogotsi, Science 372 (2021) eabf1581.
[16] M. Naguib et al., Adv. Mater. 23 (2011) 4248–4253.
[17] V.K. Chauhan et al., Adv. Eng. Mater. 26 (2024) 2301962.
[18] W. Zeng et al., Adv. Mater. 26 (2014) 5310–5336.
[19] T.S. Mathis et al., ACS Nano 15 (2021) 6420–6429.
[20] K. Maleski, V.N. Mochalin, Y. Gogotsi, Chem. Mater. 29 (2017) 1632–1640.
[21] S. Uzun et al., Adv. Funct. Mater. 29 (2019) 1905015.
[22] S. Uzun et al., Small 17 (2021) 2006376.
[23] L. Bi et al., Adv. Funct. Mater. 34 (2024) 2312434.
[24] M.R. Islam et al., Adv. Sci. 11 (2024) 2304140.
[25] B. Akuzum et al., ACS Nano 12 (2018) 2685–2694.
[26] S. Abdolhosseinzadeh et al., Adv. Mater. 32 (2020) 2000716.
[27] Y. Shao et al., Nat Commun 13 (2022) 3223.
[28] L. Bi et al., Adv. Funct. Mater. 3 (2024) 2312434.
[29] Q.-T. Lai et al., Small 19 (2023) 2300283.
[30] R. Garg et al., Small Methods 7 (2023) 2201318.
[31] X. Su et al., Appl. Surf. Sci. 639 (2023) 158205.
[32] M. Downes et al., Nat. Protoc. 13 (2024) 1807–1834.
[33] K. Shevchuk et al., Chem. Mater. 35 (2023) 8239–8247.
[34] M. Shekhirev et al., Prog. Mater Sci. 120 (2021) 100757.
[35] C.J. Zhang et al., Chem. Mater. 29 (2017) 4848–4856.
[36] J. Orangi et al., ACS Nano 14 (2019) .
[37] T. Seckler, K. Jagielski, D. Stunder, Int. J. Environ. Res. Public Health 12 (2015) 5886–5904.
[38] A. Inman et al., J. Mater. Res. 37 (2022) 4006–4016.
[39] N. Driscoll et al., Sci. Transl. Med. 13 (2021) eabf8629.
[40] C. Kim, et al., in: 2024 IEEE 7th International Conference on Soft Robotics (RoboSoft), 2024, pp. 1075–1081.